Australasian Physical & Engineering Sciences in Medicine (2019) 42:981–993
https://doi.org/10.1007/s13246-019-00797-8

SCIENTIFIC PAPER

Analysis of hypoxia in human glioblastoma tumors with dynamic 18F-FMISO PET imaging

Redha-alla Abdo[1] · Frédéric Lamare[2,3] · Philippe Fernandez[2,3] · M'hamed Bentourkia[1]

Received: 23 May 2019 / Revised: 27 August 2019 / Accepted: 31 August 2019 / Published online: 13 September 2019

Abstract

Gliomas are the most common type of primary brain tumors and are classified as grade IV. Necrosis and hypoxia are essential diagnostic features which result in poor prognosis of gliomas. The aim of this study was to report quantitative temporal analyses aiming at determining the hypoxic regions in glioblastoma multiforme and to suggest an optimal time for the clinical single scan of hypoxia. Nine subjects were imaged with PET and 18F-FMISO in dynamic mode for 15 min followed with static scans at 2, 3 and 4 h post-injection. Spectral analysis, tumor-to-blood ratio (TBR) and tumor-to-normal tissue ratio (TNR) were used to delimit perfused and hypoxic tumor regions. TBR and TNR images were further scaled by thresholding at 1.2, 1.4, 2 and 2.5 levels. The images showed a varying tumor volume with time. TBR produced broader images of the tumor than TNR considering the same thresholds on intensity. Spectral analysis reliably determined hypoxia with different degrees of perfusion. By comparing TBR and TNR with spectral analysis images, weak to moderate correlation coefficients were found for most thresholding values and imaging times (range: 0 to 0.69). Hypoxic volume (HV) estimated from the net uptake rate (K_i) were changing among imaging times. The minimum HV changes were found between 3 h and 4 h, confirming that after 3 h, there was a very low exchange of 81F-FMISO between blood and tumor. On the other hand, hypoxia started to dominate the perfused tissue at 90 min, suggesting this time is suitable for a single scan acquisition irrespective of tumor status being highly hypoxic or perfused. At this time, TBR and TNR were respectively found in the nine subjects as 1.72 ± 0.22 and 1.74 ± 0.19.

Keywords Hypoxia · Glioblastoma · Spectral analysis · 18F-FMISO · Tumor-to-blood ratio · PET imaging

Introduction

Glioma tumors are the most common type of primary brain tumors. Among all glioma tumors, glioblastoma multiforme (GBM) accounts for 60–70% [1]. Based on some histopathological studies, GBM consists of poorly differentiated astrocyte cells, nuclear atypia, mitotic activity, diminished apoptosis, neo-angiogenesis, necrosis and hypoxia [2, 3]. The high levels of hypoxia (insufficient oxygen supply) and the great heterogeneity in GBM result in poor prognosis. Therefore, this reduction of oxygen does not shrink the tumor since GBM can develop biological processes which lead to survival in hypoxic condition. The most commonly used imaging technique for GBM tumor hypoxia is Positron Emission Tomography (PET) with 18F-FMISO [4]. Earlier studies demonstrated that 18F-FMISO is trapped in highly hypoxic tumors till 4 h post-injection [2, 5]. 18F-FMISO was found to be correlated with pO_2 polarography while the mostly used radiotracer 18F-fluorodeoxyglucose (18F-FDG) was reported to not reliably differentiate hypoxic from normoxic tumors [6]. On the other hand, Toyonaga et al. reported that 18F-FDG uptake in a hypoxic tumor would reflect viable tumor volume [7]. In fact they showed that a tumor volume as defined on an MRI-FLAIR image was occupied with 18F-FDG uptake mostly in the surrounding of the tumor, and 18F-FMISO occupying the inner part of the tumor reflecting hypoxia, but there is a common zone occupied by both radiotracers. It is well recognized that extended hypoxia produces necrosis, and necrosis is a good indicator

✉ M'hamed Bentourkia
mhamed.bentourkia@usherbrooke.ca

[1] Department of Nuclear Medicine and Radiobiology, Université de Sherbrooke, 3001, 12th Avenue North, Sherbrooke, QC J1H 5N4, Canada

[2] Service de Médecine Nucléaire, Avenue du Haut-Lévêque, 33604 Pessac Cedex, France

[3] Université de Bordeaux-II, EPHE, 33076 Bordeaux, France

of tumor aggressiveness and poor prognosis. In another paper, Toyonaga et al. showed that a tumor-to-normal cerebellum ratio of 1.67 from 18F-FMISO images can predict tumor necrosis with high sensitivity and specificity [8].

The determination of tumor hypoxia allows appropriate therapy management such as the increase of the radiotherapy dose to the hypoxic regions, or modifying the chemotherapy treatment dose [9, 10]. Currently, few methods are used to quantify the hypoxic volume. The earlier techniques were based on the use of the relative delineation of tumor hypoxia using a reference tissue such as normal tissue or a volume of blood. Tumor-to-blood ratio (TBR) and tumor-to-normal contralateral (or nearby the tumor) tissue ratio (TNR) are the most common metrics used to quantify tumor hypoxia. Several threshold values of TBR and TNR exist in the literature. A TBR threshold value of 1.2 became the standard in most studies [11-13]. In imaging, most of the previous studies used static PET acquisitions. Casciari et al. reported the analyses of 18F-FMISO dynamic images and developed a kinetic model for the metabolism of 18F-FMISO [14]. This model aimed to estimate the rate constants which control the transport of 18F-FMISO in the tumor with homogenous oxygen consumption. Thorwarth et al. proposed a new kinetic model for 18F-FMISO which included the blood volume, the diffusive and the accumulative compartments within the tumor [5]. They found that no single ratio of standardized uptake values (SUV) may be sufficient to accurately define the hypoxic volume. Other kinetic models have been reported such as in [15, 16].

It has been demonstrated that hypoxia image varies in volume as a function of time depending on its location to the blood vessels, and it has also been identified as having subtypes influencing therapy prognosis [17-19]. Furthermore, Grkovski et al. reported that scans at later times after 18F-FMISO injection such as at 2 h to 4 h do not provide information on tumor perfusion and thus on hypoxia subtypes [20]. They proposed a 20 min dynamic 18F-FMISO scan to be sufficient in the clinic. The slow diffusion of 18F-FMISO affects the determination of the steady-state time at which to proceed with the calculation of TBR and TNR [21]. On the other hand, the pharmacokinetic modeling with the usual two-tissue compartments has been applied with 18F-FMISO in order to assess hypoxia [5, 16, 19, 20]. Basically, this type of analysis on the pixel basis generates noisy images as demonstrated in the parametric image of the rate constant k_3 [19, 20], or the application of the two-tissue compartment model designed to homogeneous tissues to be used in heterogeneous tissues as in GBM [22]. In addition, the fact that constraining image pixels into two compartments, ignoring the subtypes of hypoxia, introduces uncertainties on hypoxia determination [17].

Spectral analysis approach can be considered as compartmental analysis but without any constraint (unlimited exponential functions), to finally provide images of any degree of hypoxia. Since each image voxel can be decomposed into its physiological contributions, this allows the production of images of hypoxia subtypes and, for example, to differentiate GBM from less malignant gliomas. Another advantage of spectral analysis is that the uncertainty on the input function is minor since the images are extracted from the frequencies of the basis functions not from the intensities. Finally, spectral analysis can be used without an a priori imposed model or any prior configuration [22]. Since the introduction of spectral analysis in the field of nuclear medicine, it has been validated with standard methods such as compartmental modeling. The rate constants from compartmental modeling were compared with spectral analysis in a 11C-acetate kinetic model [23]. Murase et al. used technetium-99m hexamethylpropylene amine (99mTc-HMPAO) to quantify the brain perfusion index. They suggested that spectral analysis provides a more reliable BPI which is directly proportional to cerebral blood flow [24]. The reader can find more applications of spectral analysis in comparison with compartmental modeling in these references [23, 25-27] and on spectral analysis uncertainties in [28].

Either for spectral analysis or compartmental modeling, blood samples are required for dynamic analysis to determine the input function (IF). IF can be determined using various techniques. Manual withdrawal blood sampling is the most reliable method for determining IF. However, this method is cumbersome, risky and time-consuming. Therefore, several methods were developed to overcome the difficulty of manual sampling such as automatic sampling using automatic blood pumping, population-based input function using only one blood sample, and Image-based input function (IBIF). De Geus et al. found that IBIF is accurate and can replace arterial blood sampling [29]. They compared IBIFs extracted from the left ventricle, the descending aorta and the abdominal aorta with IF obtained from blood sampling and the correlation was above 94% for all three IBIFs. Grecchi et al. used IBIF with spectral analysis to estimate the kinetic parameters in acute lung injury [30], while Silvestri et al. used IBIF with spectral analysis in lung cancer [31]. Factor analysis estimation of blood from the PET images has shown some popularity in image analysis. Boutchko et al., estimated the blood curves from PET images using clustering-initiated factor analysis [32]. Another study used factor analysis to estimate the blood component in recurrent high-grade glioma [33]. The noise in IF can be reduced by fitting the rising part of IF with polynomials and the decaying part with exponentials [34]. This method can even enhance the IF by finding the maximum which could be missed due to the time sampling. This maximum is defined at the intersection of the polynomial function and the set of exponentials [34].

Another effect to mention is the partial volume effect (PVE). PVE is recognized to lower the image intensity of a

small size object, i.e. comparable to scanner spatial resolution, while it spatially expands this intensity to neighboring pixels in the image. In the case of the common carotid artery imaged with 18F-FMISO, there would be no expected uptake of the radiotracer around the artery as there is no expected hypoxia. Consequently, spill-in in the artery image should be marginal. Furthermore, in this work, we were seeking the spatial determination of the tumor components, irrespective of their intensities. In this case, the shape of the components time course were the only interest.

The main aim of this study was to report the quantitative temporal analysis of the hypoxic regions in GBM tumors by means of spectral analysis in comparison to the commonly used approaches of TBR and TNR. We also suggested the optimal time to acquire a single scan after 18F-FMISO injection, which is the routine in the clinic.

Methods

Subject data

Nine subjects planned for radio-chemotherapy treatment were included in this study. All subjects were diagnosed with GBM grade IV according to the World Health Organization (WHO) classification. The scans consisted of PET with 18F-FMISO and computed tomography (CT) imaging. In addition, T1 Magnetic Resonance Imaging (MRI) weighted-image with the injection of gadolinium (64-Gd) has been acquired. This work was done with the approval by the ethics committee of the University of Bordeaux-II. The subjects signed a written informed consent for the imaging procedures.

Imaging protocols

Each subject was scanned with a PET/CT GE scanner (Discovery RX General Electric Medical System) [35]. The imaging protocol for 18F-FMISO PET was first set as a dynamic scan of 15 min after the administration of 3.7 MBq/kg of 18F-FMISO. 18F-FMISO was prepared as reported by Lim and Berridge [36]. CT was performed with 120 kVp, 80–250 mA, and a pitch of 3.6. The images were reconstructed in 12 frames of 10 s, 8 frames of 15 s and the remaining time in frames of 60 s. The same subjects were further scanned for static images of 10 min duration and acquired at 2 h, 3 h and 4 h post-injection to ensure the uptake of 18F-FMISO in the tumor (the 4 h scans were done in 3 out of the 9 subjects). The latter two or three scans were coregistered with the dynamic scans based on the coregistration of their respective CT images.

Spectral analysis

Spectral analysis technique was used to decompose the PET dynamic images into their components in order to isolate the hypoxic tissue image. Spectral analysis is a technique solving for amplitudes A_i and exponents B_i of a set of N exponentials to fit the time-activity curve (TAC) of an image pixel i (1). The set of exponentials were convolved with the blood IF and added a fraction A_{N+1} of the IF to account for blood volume in the pixel [23]. No a priori information or assumptions on the number of exponentials were required, which is one of the strength of spectral analysis. Kinetic components, amplitudes and rate constants can be estimated from the amplitudes and the exponents (or frequencies) of the exponentials fitting the pixels time course. The outputs of spectral analysis can be related to specific tracer's physiological properties. The main equation of spectral analysis is given as:

$$TAC(t) = \left[\sum_{i=1}^{N} A_i e^{-B_i t}\right] \otimes IF + A_{N+1} IF \quad (1)$$

A and B (1) were assumed to have real non-negative values. The B values were chosen to be between 10^{-5} and 1 [23]. This range would reflect the possible values of the physiological processes. We also used the B values as reported in [22] ranging from $1/(3 \times TE) = 1/(3 \times 180 \text{ min}) = 0.00185 \text{ min}^{-1}$ where TE was the end time of the study, and $3/TI = 3/(10\text{s}/60\text{s}) = 18 \text{ min}^{-1}$ where TI was the 10 s duration of the first frame. The calculations gave similar results (see in section of Results). The number of exponentials was set to $N = 100$. The accumulating component at $B = 0$ was added explicitly to the frequency grid. Blood volume was located one step after the highest B value and its amplitude was identified as A_{N+1}. Non-negative least square method was used to estimate the A values [23]. As a result, each pixel was decomposed into its basis functions (exponential functions) and around 1 to 5 components were found for each pixel, and these components were identified with their pair of (A, B) values.

Estimation of the accumulating coefficient A_0 at low values of B was affected by noise in the pixels time course. Therefore, three filtering approaches have been used in the literature to improve the estimation of the coefficient A_0 [37]. In this work, we applied one of the three approaches which eliminated the exponentials below the cutoff frequency of $1/180$ min [37]. The selection of this filtering was based on the best correlation of the fit obtained with these methods and tumor TAC.

The output of spectral analysis can be connected to some physiological parameters as indicated by Gunn et al. [38]. These parameters are the blood-to-tissue rate

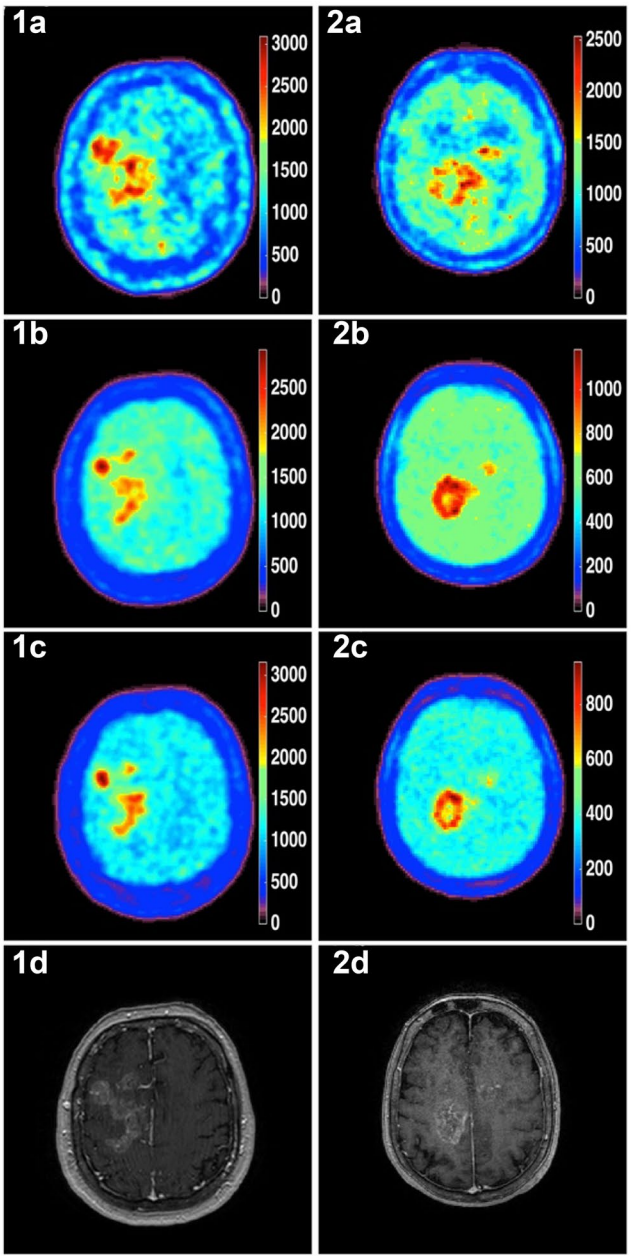
1a
2a
1b
2b
1c
2c
1d
2d

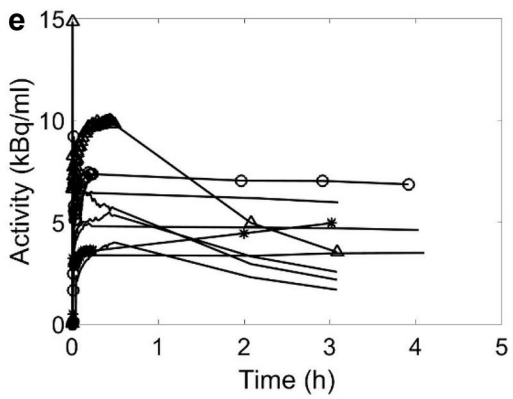
e
Activity (kBq/ml)
Time (h)

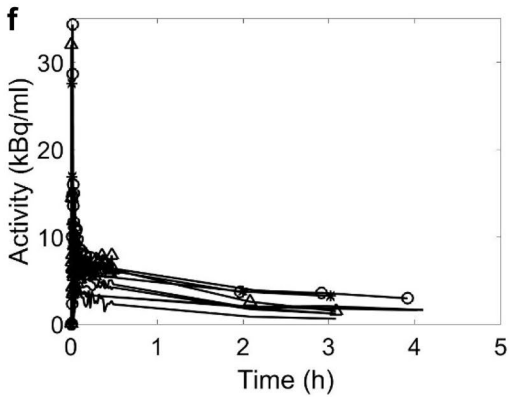
f
Activity (kBq/ml)
Time (h)

◂**Fig. 1** Progress of 18F-FMISO retention in the tumor. 1**a**–1**d** Subject-2 and (**2a**–**2d**) Subject-9 images. Frame times for **a**–**c** were 15 min, 2 h and 3 h respectively. **1d** and **2d** the corresponding MRI images. **e** TACs of the tumors in the nine subjects. **f** TACs of the blood from the carotid ROI in the nine subjects. The curve with a circle marker is from Subject-2 and that with a triangle marker is from Subject-9. The TAC with a star marker is the only continuously increasing curve

constant K_1, the net uptake constant of the tracer K_i, and the distribution volume. In this study, we calculated the 18F-FMISO $K_i = K_1 \times k_3/\left(k_2 + k_3\right)$ as equal to the amplitude A_0 at $B = 0$ [26]. The calculated values of A and B for each component in each pixel allowed to reconstruct the parametric images which can be further used to investigate the tracer behavior for the specific physiological processes. A parametric image can be made with: (1) any single value or an interval of values of A_i or B_i at the corresponding pixel in the image; (2) by forming the pixel value with the value of the exponential made with a single or an interval of values of A_i and B_i such as $A_i \ \exp\left(-B_i t\right)$. This exponential is called tissue impulse response function or the basis function. It is worth noting that, from the basis functions, dynamic images for any desired time can be derived; (3) by convolving the basis functions with the input function to obtain pixel TACs for any component. The whole brain can be parametrized, excluding non-brain structures.

Image analysis

All the analyses were implemented in MATLAB (R2015b, The MathWorks Inc, Natick, MA, USA). The blood IF was derived from the common carotid artery in PET images by means of a region of interest (ROI) drawn on the sagittal view to encompass a large area of the carotid which was less prone to PVE. Another ROI was drawn on the normal contralateral tissue with the help of MRI images. The ROIs on the tumors and on the common carotid were drawn by means of active contours. TBR images were obtained by dividing the 18F-FMISO images by the blood value from IF at the corresponding frame times. Similarly, TNR images were obtained by dividing the 18F-FMISO images by the contralateral tissue TAC at the corresponding frame times. Multiple fixed threshold values on TBR and TNR image intensity as 1.2, 1.4, 2 and 2.5 were used for thresholding the images to isolate hypoxic volume.

The spectral analysis parametric images were compared with TBR and TNR images using Pearson's correlation. Besides, we calculated the hypoxic volume from TBR, TNR and K_i spectral analysis images.

Results

Tumor assessment with TBR and TNR

An example of PET images at 15 min, 2 h and 3 h in two subjects are shown in Fig. 1 together with their corresponding MRI images and their tumor and blood TACs. In comparison to the other PET images and to MRI images, the images at 15 min located the tumor, but without clear delineation, even tissue and blood were still exchanging the radiotracer in the whole brain. The regions of the tumor already showed a higher intensity than the rest of the brain. The accumulation of 18F-FMISO was still changing even after 2 h and 3 h and the tumor on the MRI image presented different diffusion. In these two subjects, the uptake of 18F-FMISO presented different time courses as depicted in Fig. 1e. In Subject-9, although the tumor was well defined at 3 h with respect to 15 min or even to 2 h, its TAC declined at later frame times without affecting the tumor contrast (Fig. 1e). These two subjects presented different TACs and they were typical of the other subjects analyzed in this study.

Figure 2 shows a sagittal slice from Subject-2 encompassing the common carotid artery on which an ROI was drawn to determine the IF, together with its corresponding blood and tissue component images derived with factor analysis. Their TACs were plotted in Fig. 2d where the contribution from the tissue component was marginal in this ROI. In average the real size of the common carotid arteries are > 6 mm in men and women, and the transaxial and axial spatial resolution (full width at half maximum) of the scanner used in this study were respectively 5.1 mm and 4.8 mm [35], thus, the ROI was partially affected by PVE and this had an impact on TBR but not on spectral analysis since the spectral analysis component images were extracted based on the frequencies B_i. In the rest of this paper, we used the IF derived from the measured images.

Figure 3 shows how the threshold values of 1.2, 1.4, 2 and 2.5 isolated the tumor hypoxic volumes in TBR and TNR at 3 h frame images. The TBR thresholded images showed a large volume of normal tissue at threshold values of 1.2 and 1.4. At the larger threshold values of 2 and 2.5, the volume of normal tissue in TBR was almost removed. The broad regions defined with TBR can be explained by the fact that radioactivity in blood was generally low with respect to normal tissue, and also the underestimation of the activity in blood as defined from the carotid artery might be partly due to the partial volume effect. However, TNR was more adequate in isolating the high uptake in the tumor especially at the threshold of 1.4. This result was expected since the contralateral ROI should have similar uptake in the whole brain excepting the hypoxic tumor.

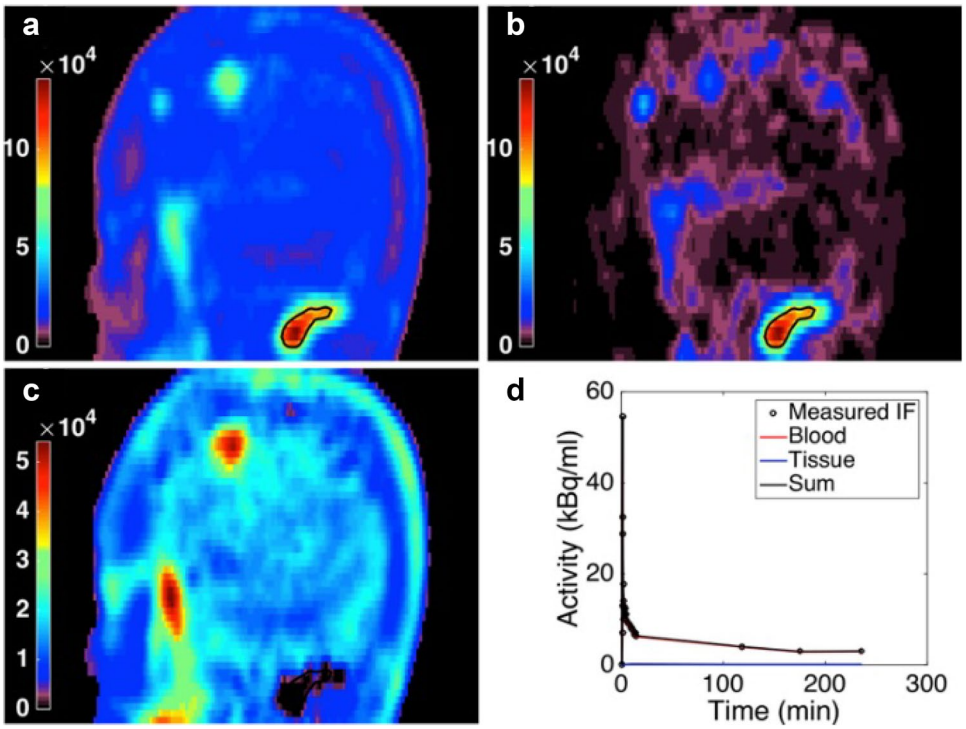

Fig. 2 **a** Sagittal slice showing the common carotid artery in the measured image. **b** and **c** Are the blood and tissue images as defined with factor analysis. **d** Plots of the blood TACs derived from the ROIs on the carotid arteries defined in **a**–**c**. The curve Sum is the sum of blood and tissue TACs fitting the measured TAC

In Fig. 4, the standard 1.2 threshold value using TBR and TNR images at different frame times of 15 min, 2 h and 3 h post-injection were used to delineate the tumor. The results highlighted the difference in tumor volume determination which was continuously varying. Such assumptions can lead to different results depending on the imaging time. The 15 min image shows a sparse shape of the tumor which makes it not useful for TBR or TNR analysis. At 3 h with TBR, the tumors were not isolated in the images, because, apparently, the blood component as determined from the carotid artery was too low. Consequently, TNR appeared more appropriate to delineate the tumor.

Figure 5 depicts the plots of the TACs from the nine subjects divided by the blood TACs taken from the carotids, assuming these ratios were accounting for TBR (Fig. 5a). In Fig. 5b the tumor TACs were divided by the reference tissue TACs, assuming to represent TNR. The horizontal lines in the figures indicate the 4 thresholding levels. In all subjects, the ratios exceeded the level 1.2 for TBR at 3 h, while this was not the case for the other levels of 1.4, 2 and 2.5 and for the other imaging times like at 2 h. Because the ROIs were an average over the selected pixel intensities, the results in Fig. 5 were slightly different from those in Figs. 3 and 4 where only the pixels exceeding the thresholding levels were displayed, and these pixels were not forming the whole ROI around the tumor.

Tumor assessment with spectral analysis

The comparison between the two methods based on B ranging from 10^{-5} to 1 and that ranging from 0.00185 to 18 [22] from Subject-2 was displayed in Table 1. First it can be noted that the B ranges from method 1 are contained in those of method 2. As expected, the obtained components appeared similar except that the small differences were due to the difference in the sampling of the B values. The blood component assessed at B_{N+1} had the same contribution in both methods. In the rest of this work we used method 1 with B ranging from 10^{-5} to 1.

Figure 6 shows the frequencies B_i and amplitudes A_i as calculated with spectral analysis in a single slice of the dynamic images encompassing the tumor in Subject-2. An automatic threshold set with active contours was first defined on the brain images to exclude the background. In this slice, there were 10,202 pixels. The maximum number of components per pixel in this slice was 5 including the blood component. Figure 7 presents an image slice from Subject-4 with the three components calculated with spectral analysis, i.e. the perfused, the accumulating, and the blood images. In this figure, the measured image was displayed from the 3 h acquisition while those extracted with spectral analysis were summed over the whole acquisition time from 0 to 3 h.

Figure 8 shows the reconstructed K_i images estimated from spectral analysis compared to the measured PET for two subjects. The K_i images at 15 min did not define the

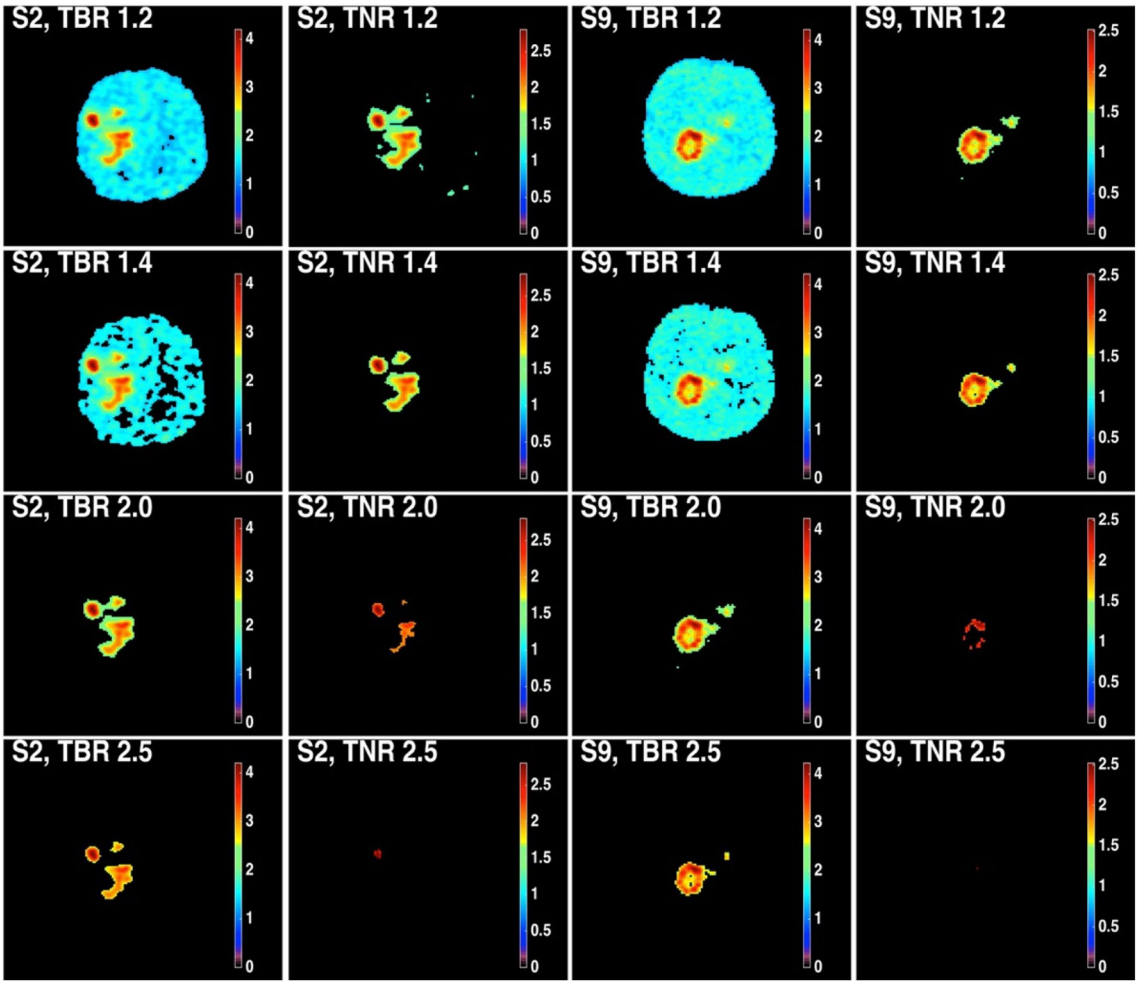

Fig. 3 Comparison of TBR and TNR images at 3 h with the four thresholding values of 1.2, 1.4, 2 and 2.5 from top to bottom rows, respectively. The left two-column images are for Subject-2 (S2) and the right are for Subject-9 (S9). TNR appears more appropriate to segment hypoxia than TBR

tumor volume for both subjects. At 2 h, a few pixels in the tumor were expressed compared to 15 min. The 3 h image showed a comparable shape to the measured tumor.

The comparison of spectral analysis images at the pixel basis with TBR and TNR is shown in Table 2 to indicate the best static thresholds and imaging times that can match the dynamic results. Table 2 showed weak to moderate correlation coefficients for most thresholding values and imaging times (range: 0 to 0.69). Table 3 shows the estimated hypoxic volume changes between two consecutive imaging times determined from the accumulating component obtained with spectral analysis. The mean HV changes were high between the 15 min and 2 h and 2–3 h (21.7% ± 21% and 29.2% ± 18.3%, respectively). While, the mean HV changes between 3 and 4 h was very low.

Determination of the optimal time for a single static scan

For this analysis, the images of the spectral analysis accumulating component representing hypoxia were reconstructed at steps of 1 min from 0 to 180 min, from which were extracted the TAC of the tumor using the ROI drawn on the tumor at 180 min in the measured image. The TAC of the carotid blood and that of the contralateral normal tissue were obtained from the measured images and interpolated from 0 to 180 min. The intersection of the accumulating TAC with those of carotid blood and contralateral tissue determined the minimum of the optimal time at which hypoxia starts dominating the rest of tissue images. This approach is more suitable than what is usually reflected by

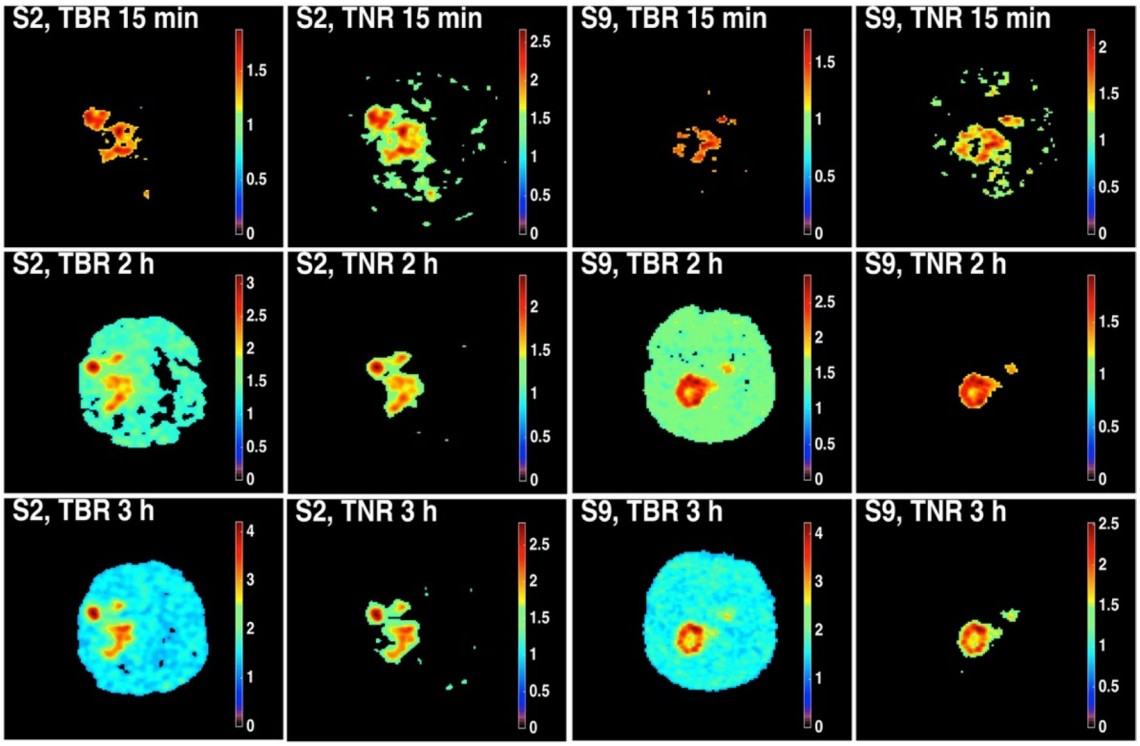

Fig. 4 Delineation of tumor volume at 15 min (top row), 2 h (middle row) and 3 h (bottom row) for the 1.2 thresholding value using TBR and TNR. The two columns on the left are respectively for TBR and TNR in Subject-2 (S2), and the two right columns are for TBR and TNR in Subject-9 (S9)

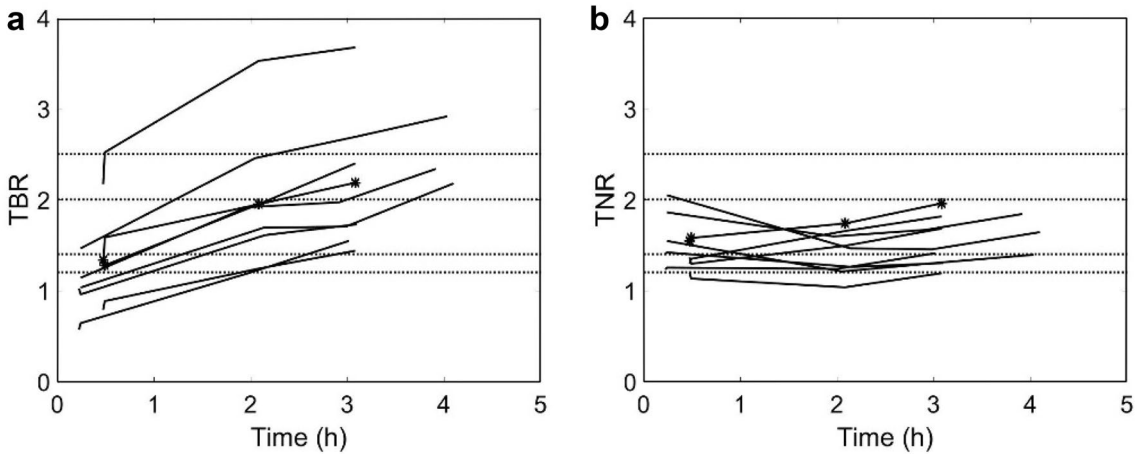

Fig. 5 Plot of tumor TACs divided by IFs (**a**) and by the reference tissue TACs (**b**) in the nine subjects. Only the last frames were displayed. The curves with stars correspond to the uniformly increasing TAC (Fig. 1e). The levels of 1.2, 1.4, 2 and 2.5 were also plotted as horizontal dotted lines. The curves from the nine subjects have TBR greater than 1.2 at 3 h, but not all of them have values above the other levels. The time lag between the curves was due to the fact of subject dynamic imaging for 15 min or 30 min, and of static scans at 3 h or 4 h post-injection

TBR and TNR measured in a single scan at a given time of 2 h or 3 h, multiplied by factors (see Figs. 3 and 4). Table 4 shows the minimum of the optimal times for a single static scan in the nine subjects. The mean over the nine subjects of the minimal optimal time for the single scan was found at 89 ± 59 min and 105 ± 69 min, with respect to blood and contralateral normal tissue, respectively. The large deviation in these values depended on the shape of tumor TACs

Table 1 Comparison of spectral analysis A and B values extracted from tumor TAC of Subject-2 with B ranging from 10^{-5} to 1 versus B ranging for 0.00185 to 18 [22]. The number of components and their parameter values were nearly similar

Component number	B range: 10^{-5} to 1		B range: 0.00185 to 18	
	A	B	A	B
1	0.0005	0	0.0005	0
2	0.0026	0.0977	0.0029	0.0999
3	0.0067	0.1748	0.0049	0.1742
4	0.0020	0.1963	0.0036	0.1911
5	0.1775	1 + step	0.1775	18 + step

where some tumors were more hypoxic (increasing TACs) than perfused (decreasing TACs). The shape of the TACs was indicated in column 1 of Table 4 (see also Fig. 1e). At the time of 89 min, TBR and TNR were shown in Table 4 and their means over the nine subjects were 1.72 ± 0.22 and 1.74 ± 0.19. By assuming that these values of TBR and TNR provided enough contrast of hypoxia image, the minimal optimal time was then suggested to be 90 min irrespective of tumor status as being more hypoxic or more perfused. The minimum of optimal times of 90 min was defined based on the analysis of TACs, where the hypoxia pixel intensity was averaged. In order to determine the hypoxia extent within the tumor, in terms of pixels, TNR of the single image acquired at 90 min with levels of 1.2 or 1.4 could isolate the hypoxia as in Figs. 3 and 4.

Discussion

The most important challenge in determining the hypoxic region in 18F-FMISO images is that the accumulating activity in the pixel depends on the volume of hypoxia in the tumor, the transport properties, the imaging protocols and noise characteristics. Most PET studies with 18F-FMISO

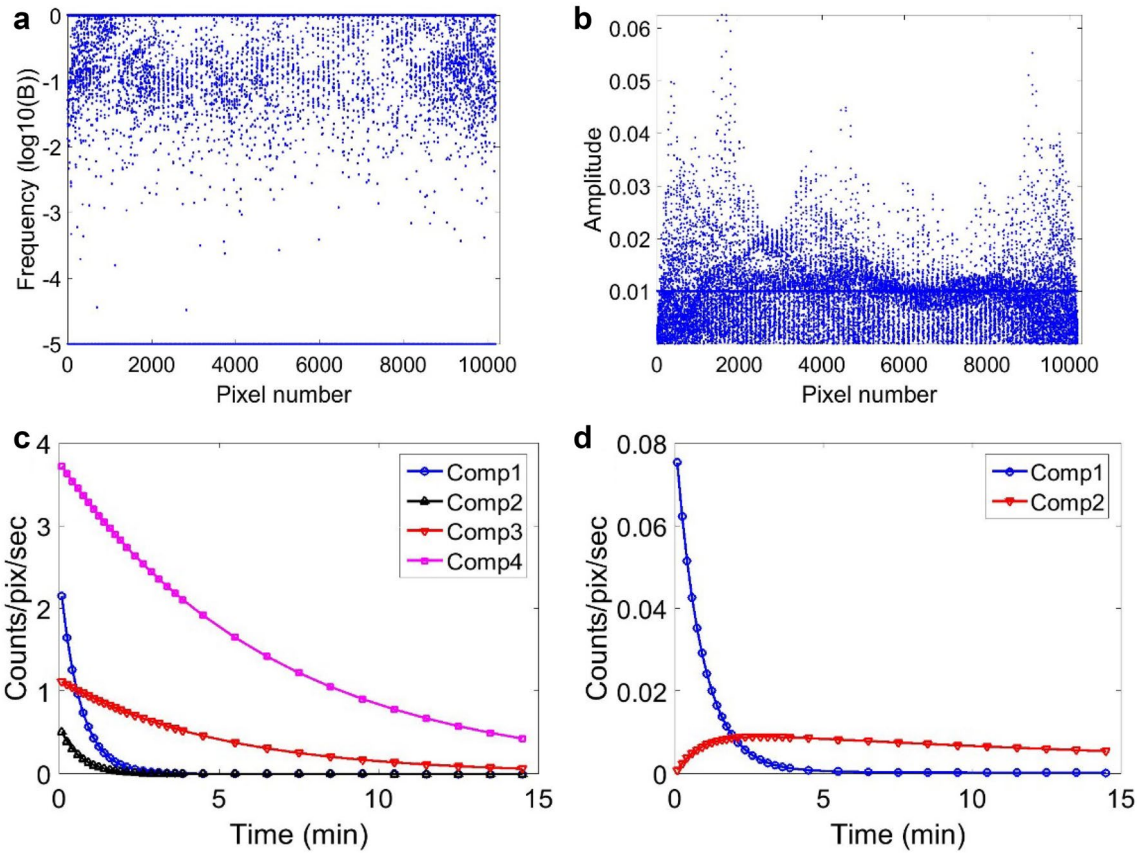

Fig. 6 Distribution of frequencies (**a**) and amplitudes (**b**) in a single slice from Subject-2 including the tumor. **c** Spectral analysis tissue response functions from a single pixel from this slice. The total number of pixels fitted excluding the background was 10,202. The maximum number of components observed in a pixel was 5. **d** Tissue response functions of a single pixel as defined with two-tissue compartmental modeling. The y-axis in **a** was used to select the frequency band, and all pixels having frequencies in that band formed that component image. The corresponding amplitudes were taken from **b** to form, for each pixel, the sum over the B_i frequencies in the band $\sum_i A_i \exp\left(-B_i t\right)$.

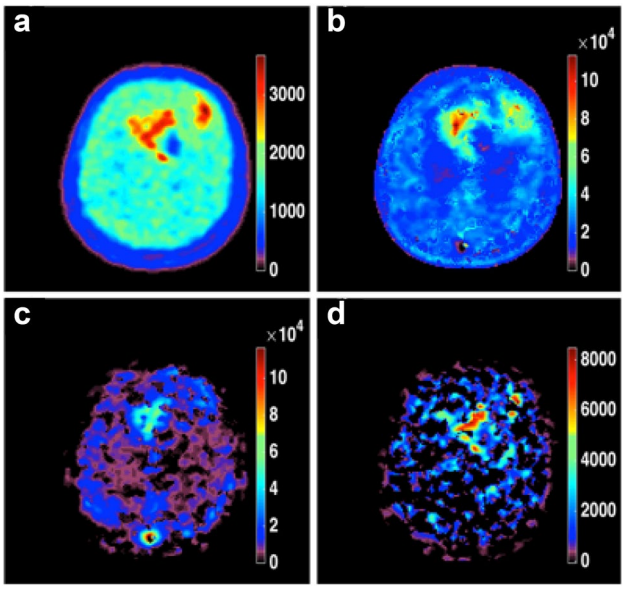

Fig. 7 Images from Subject-4 showing in **a** a measured slice. In **b–d** images from spectral analysis of perfused tissue, blood and hypoxia. The images in **b–d** were summed over their time frames

hypoxia employ a single static scan at a later time such as at 2–4 h post-injection to allow accumulation of 18F-FMISO in the tumor, and removal of 18F-FMISO from blood and perfused tissues. The images are then acquired for 10–20 min.

Common assessments of hypoxia are mean and maximum SUV, TBR and TNR which are well suited for static PET scans. The present study showed that the quantification of tumor hypoxia with TBR or TNR were dependent on the time of the measurement which was not standard between individuals. This observation is clearly apparent in Fig. 1 where the tumor hypoxia distribution is continuously changing with time. If one wants to give a boost of radiation during radiotherapy treatment to the hypoxic region, the decision would depend on the scanning time of 18F-FMISO.

The threshold limit on TBR or TNR has not yet been well established although the value of 1.2 is commonly used. In the literature, many threshold values have been used for delineating or calculating the hypoxic volume. In addition to the varying accumulation of 18F-FMISO in the tumor with time, the uncertainties on the 18F-FMISO activity in blood and in the normal tissue have a non-negligible impact on hypoxia determination as demonstrated in Figs. 3 and 4.

By observing the images of Fig. 3, it appears that the determined activity in normal tissue was high in comparison to blood activity which resulted in nearly no background removal in TBR at the thresholds of 1.2 and 1.4 in both subjects at 3 h, while TNR approach was more efficient to isolate the tumor. For a threshold of 1.2 in Fig. 4, the blood activity was high at 15 min and was comparable to normal tissue activity, but less than the activity in some regions of the tumor (see TBR columns). At later time points, the blood activity decreased more rapidly than the activity in tissue. With TNR and still at a threshold of 1.2, the accumulation of 18F-FMISO in the tumor was more pronounced at 2 h and above.

In order to acquire dynamic images, the measurements become lengthy which makes them uncomfortable for the

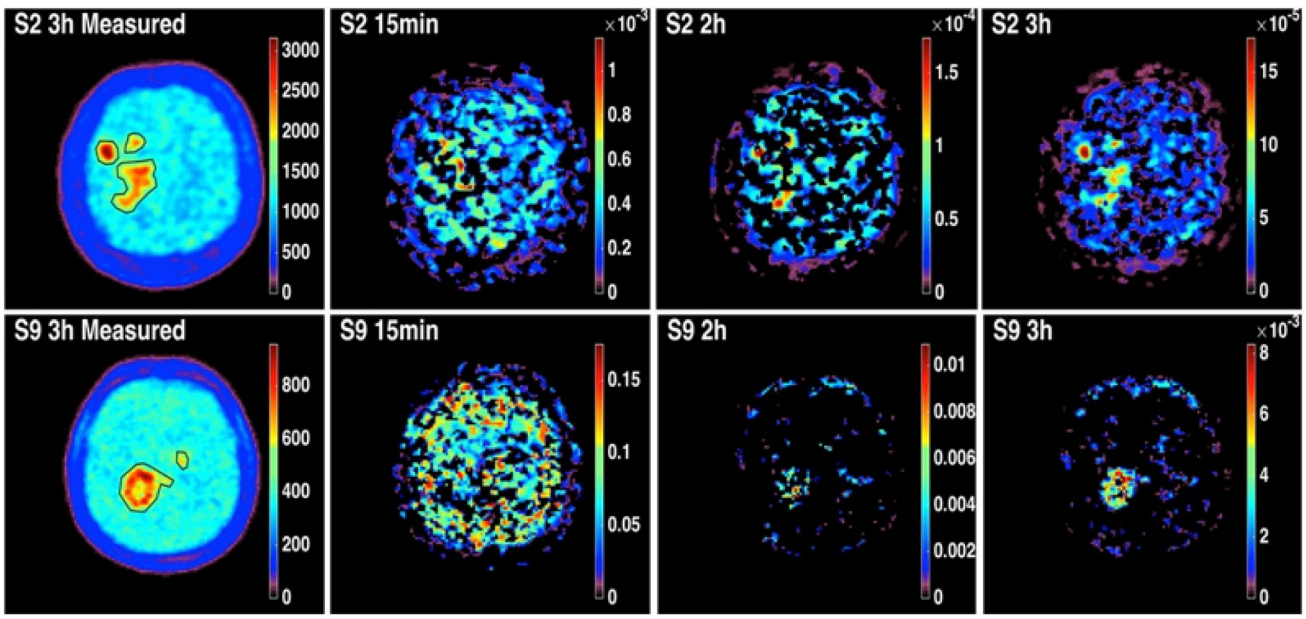

Fig. 8 Images from spectral analysis for Subject-2 and Subject-9. The first column are the measured PET images. Columns (2–4) are K_i parametric images estimated by spectral analysis at 15 min, 2 h, and 3 h

Table 2 Correlation coefficients of the comparison between whole image pixels obtained with TBR and TNR vs spectral analysis

Method	15 min	2 h	3 h
TBR at th = 1.2	0.30 ± 0.16	0.29 ± 0.11	0.40 ± 0.12
TBR at th = 1.4	0.22 ± 0.22	0.42 ± 0.16	0.53 ± 0.15
TBR at th = 2.0	0.05 ± 0.15	0.36 ± 0.20	0.67 ± 0.15
TBR at th = 2.5	0.01 ± 0.04	0.00 ± 0.00	0.00 ± 0.00
TNR at th = 1.2	0.33 ± 0.14	0.44 ± 0.14	0.69 ± 0.11
TNR at th = 1.4	0.35 ± 0.16	0.45 ± 0.18	0.69 ± 0.14
TNR at th = 2.0	0.00 ± 0.00	0.09 ± 0.17	0.25 ± 0.35
TNR at th = 2.5	0.00 ± 0.00	0.00 ± 0.00	0.00 ± 0.00

th threshold

Table 3 Deviation percentages ($100 \times |(Npix(t1) - Npix(t2))|/(Npix(t1) + Npix(t2))$) of hypoxic volume ($K_i$) changes between two consecutive imaging times. $Npix(t)$ was the number of pixels in the tumor ROI at time t

Subject	15 min to 2 h	2–3 h	3–4 h
S1	26.4	29.8	0.6
S2	16.6	17.4	0.2
S3	1.7	19.7	–
S4	1.9	14.6	0.1
S5	7.8	6.1	–
S6	12.8	43.4	–
S7	39.2	35.1	–
S8	67.7	67.7	–
S9	26.4	29.8	–
Mean ± STD	21.7 ± 21.0	29.2 ± 18.3	0.3 ± 0.2

subject, with the need of accurate repositioning of the subject in the scanner for the different imaging sessions and of an accurate image coregistration. The benefit is that dynamic images allow a better decision on the presence of hypoxia either by kinetic modeling or by algorithms such as spectral analysis. Spectral analysis is more flexible than compartmental analysis in the sense that it does not impose constraints on the time course of the pixels, while compartmental analysis imposes rigid behavior (compartments) to the circulation of the radiotracer, and to tissue homogeneity. By observing the spectral analysis images in Fig. 8, it can be concluded that the 15 min and the 2 h did not define well the tumor volume. The 3 h spectral analysis image showed a comparable shape to the measured PET image. By comparison of spectral analysis to TBR and TNR, it was difficult to find a precise limit for optimum static imaging time. However, only the 3 h images with TNR at thresholds 1.2 and 1.4 and TBR at threshold 2 have a moderate correlation coefficient (around 0.70). The estimated changes in HV between two consecutive times very slightly varied between 3 h and 4 h, while the other times had high variations in tumor volume. Therefore, the 3 h imaging time for static 18F-FMISO imaging provided the best contrast of hypoxia. However, the 90 min scan achieved an acceptable contrast of the tumor of 1.72 ± 0.22 and 1.74 ± 0.19 as respectively defined with TBR and TNR (Table 4). Finally, a single scan at 90 min with TNR applied at levels of 1.2 or 1.4 were demonstrated in this work to be optimal to isolate hypoxia.

We note, however, that the small sample size (9 subjects) was considered the main limitation in the current study. More subjects with different status of the tumor as perfused and hypoxic should reduce the variability in the frequency delimitation of hypoxic volumes, and consequently

Table 4 Minimum of optimal single scan times in the 9 subjects deduced from tumor ROI at 180 min (columns 3 and 4). Also are shown TBR and TNR at 89 min and 180 min. The value 0 means the curves did not intersect and the hypoxia was well discriminated. TBR and TNR were respectively calculated as measured tumor TAC/carotid blood TAC and measured tumor TAC/contralateral tissue TAC at 89 min and 180 min

Subject	Tumor TAC shape	Hypoxia versus blood (min)	Hypoxia versus normal tissue (min)	TBR 89	TNR 89	TBR 180	TNR 180
S1	—	142	195	1.90	1.97	2.89	2.02
S2	⟍	103	130	2.09	1.94	3.37	2.22
S3	⟍	107	99	1.59	1.88	2.44	2.17
S4	⟍	119	138	1.64	1.68	2.39	2.01
S5	⟍	0	0	1.48	1.53	1.96	1.6
S6	⟍	99	90	1.52	1.72	2.46	2.18
S7	⟍	0	0	1.51	1.48	1.97	1.6
S8	⟍	81	105	1.89	1.58	2.57	1.96
S9	⟍	154	185	1.86	1.91	3.19	2.07

contributes to an accurate determination of hypoxia subtypes.

Conclusions

The changes in uptake of 18F-FMISO in glioblastoma tumor over time were investigated. We found that there would be inter-subject differences when using simple quantitative techniques such as TBR or TNR. We showed that spectral analysis allows to separate the components of each pixel and to potentially identify hypoxia. By comparing the single time techniques TBR and TNR with spectral analysis, we found moderate correlation at specific thresholding values and imaging times. Besides, a time of 90 min was demonstrated to be enough to achieve an acceptable tumor contrast independently of tumor status. These findings can be used to improve the imaging protocol of 18F-FMISO.

Compliance with ethical standards

Conflict of interest The authors declare that they have no conflict of interest.

Ethical approval All procedures performed in studies involving human participants were in accordance with the ethical standards of the institutional and/or national research committee and with the 1964 Helsinki declaration and its later amendments or comparable ethical standards. This article does not contain any studies with animals performed by any of the authors.

Informed consent Informed consent was obtained from all individual participants included in this study.

References

1. Gilbert MR (2011) Recurrent glioblastoma: a fresh look at current therapies and emerging novel approaches. Semin Oncol 38(Suppl 4):S21–33
2. Hirata K, Terasaka S, Shiga T et al (2012) (1)(8)F-Fluoromisonidazole positron emission tomography may differentiate glioblastoma multiforme from less malignant gliomas. Eur J Nucl Med Mol Imaging 39:760–770
3. Zygogianni A, Protopapa M, Kougioumtzopoulou A et al (2018) From imaging to biology of glioblastoma: new clinical oncology perspectives to the problem of local recurrence. Clin Transl Oncol 20:989–1003
4. Bekaert L, Valable S, Lechapt-Zalcman E et al (2017) [18F]-FMISO PET study of hypoxia in gliomas before surgery: correlation with molecular markers of hypoxia and angiogenesis. Eur J Nucl Med Mol Imaging 44:1383–1392
5. Thorwarth D, Eschmann SM, Paulsen F et al (2005) A kinetic model for dynamic [18F]-Fmiso PET data to analyse tumour hypoxia. Phys Med Biol 50:2209–2224
6. Zimny M, Gagel B, DiMartino E et al (2006) FDG–a marker of tumour hypoxia? A comparison with [18F]fluoromisonidazole and pO_2-polarography in metastatic head and neck cancer. Eur J Nucl Med Mol Imaging 33:1426–1431
7. Toyonaga T, Yamaguchi S, Hirata K et al (2017) Hypoxic glucose metabolism in glioblastoma as a potential prognostic factor. Eur J Nucl Med Mol Imaging 44:611–619
8. Toyonaga T, Hirata K, Yamaguchi S et al (2016) (18)F-fluoromisonidazole positron emission tomography can predict pathological necrosis of brain tumors. Eur J Nucl Med Mol Imaging 43:1469–1476
9. Thorwarth D, Eschmann SM, Holzner F et al (2006) Combined uptake of [18F]FDG and [18F]FMISO correlates with radiation therapy outcome in head-and-neck cancer patients. Radiother Oncol 80:151–156
10. Eschmann SM, Paulsen F, Bedeshem C et al (2007) Hypoxia-imaging with (18)F-Misonidazole and PET: changes of kinetics during radiotherapy of head-and-neck cancer. Radiother Oncol 83:406–410
11. Yamamoto Y, Maeda Y, Kawai N et al (2012) Hypoxia assessed by 18F-fluoromisonidazole positron emission tomography in newly diagnosed gliomas. Nucl Med Commun 33:621–625
12. Kawai N, Maeda Y, Kudomi N et al (2011) Correlation of biological aggressiveness assessed by 11C-methionine PET and hypoxic burden assessed by 18F-fluoromisonidazole PET in newly diagnosed glioblastoma. Eur J Nucl Med Mol Imaging 38:441–450
13. Swanson KR, Chakraborty G, Wang CH et al (2009) Complementary but distinct roles for MRI and 18F-fluoromisonidazole PET in the assessment of human glioblastomas. J Nucl Med 50:36–44
14. Casciari JJ, Graham MM, Rasey JS (1995) A modeling approach for quantifying tumor hypoxia with [F-18]fluoromisonidazole PET time-activity data. Med Phys 22:1127–1139
15. Wang W, Georgi JC, Nehmeh SA et al (2009) Evaluation of a compartmental model for estimating tumor hypoxia via FMISO dynamic PET imaging. Phys Med Biol 54:3083–3099
16. Bruehlmeier M, Roelcke U, Schubiger PA et al (2004) Assessment of hypoxia and perfusion in human brain tumors using PET with 18F-fluoromisonidazole and 15O–H_2O. J Nucl Med 45:1851–1859
17. Koch CJ, Evans SM (2015) Optimizing hypoxia detection and treatment strategies. Semin Nucl Med 45:163–176
18. Pajonk F, Vlashi E, McBride WH (2010) Radiation resistance of cancer stem cells: the 4 R's of radiobiology revisited. Stem Cells 28:639–648
19. Preibisch C, Shi K, Kluge A et al (2017) Characterizing hypoxia in human glioma: a simultaneous multimodal MRI and PET study. NMR Biomed 30:e3775
20. Grkovski M, Schoder H, Lee NY et al (2017) Multiparametric imaging of tumor hypoxia and perfusion with (18)F-fluoromisonidazole dynamic PET in head and neck cancer. J Nucl Med 58:1072–1080
21. Taylor E, Gottwald J, Yeung I et al (2017) Impact of tissue transport on PET hypoxia quantification in pancreatic tumours. EJNMMI Res 7:101
22. Veronese M, Rizzo G, Bertoldo A et al (2016) Spectral analysis of dynamic PET studies: a review of 20 years of method developments and applications. Comput Math Methods Med 2016:7187541
23. Bentourkia M (2003) PET kinetic modeling of 11C-acetate from projections. Comput Med Imaging Graph 27:373–379
24. Murase K, Inoue T, Fujioka H et al (1999) An alternative approach to estimation of the brain perfusion index for measurement of cerebral blood flow using technetium-99m compounds. Eur J Nucl Med 26:1333–1339

25. Cunningham VJ, Jones T (1993) Spectral analysis of dynamic PET studies. J Cereb Blood Flow Metab 13:15–23
26. Bertoldo A, Vicini P, Sambuceti G et al (1998) Evaluation of compartmental and spectral analysis models of [18F]FDG kinetics for heart and brain studies with PET. IEEE Trans Biomed Eng 45:1429–1448
27. Meikle SR, Matthews JC, Cunningham VJ et al (1998) Parametric image reconstruction using spectral analysis of PET projection data. Phys Med Biol 43:651–666
28. Turkheimer F, Sokoloff L, Bertoldo A et al (1998) Estimation of component and parameter distributions in spectral analysis. J Cereb Blood Flow Metab 18:1211–1222
29. de Geus-Oei LF, Visser EP, Krabbe PF et al (2006) Comparison of image-derived and arterial input functions for estimating the rate of glucose metabolism in therapy-monitoring 18F-FDG PET studies. J Nucl Med 47:945–949
30. Grecchi E, Veronese M, Moresco RM et al (2016) Quantification of dynamic [18F]FDG pet studies in acute lung injury. Mol Imaging Biol 18:143–152
31. Silvestri E, Scolozzi V, Rizzo G et al (2018) The kinetics of (18) F-FDG in lung cancer: compartmental models and voxel analysis. EJNMMI Res 8:88
32. Boutchko R, Mitra D, Baker SL et al (2015) Clustering-initiated factor analysis application for tissue classification in dynamic brain positron emission tomography. J Cereb Blood Flow Metab 35:1104–1111
33. Wardak M, Schiepers C, Dahlbom M et al (2011) Discriminant analysis of (1)(8)F-fluorothymidine kinetic parameters to predict survival in patients with recurrent high-grade glioma. Clin Cancer Res 17:6553–6562
34. Bentourkia M, Bol A, Ivanoiu A et al (1999) A standardized blood sampling scheme in quantitative FDG-PET studies. IEEE Trans Med Imaging 18:379–384
35. Kemp BJ, Kim C, Williams JJ et al (2006) NEMA NU 2–2001 performance measurements of an LYSO-based PET/CT system in 2D and 3D acquisition modes. J Nucl Med 47:1960–1967
36. Lim J-L, Berridge MS (1993) An efficient radiosynthesis of [18F] fluoromisonidazole. Appl Radiat Isot 44:1085–1091
37. Turkheimer F, Moresco RM, Lucignani G et al (1994) The use of spectral analysis to determine regional cerebral glucose utilization with positron emission tomography and [18F]fluorodeoxyglucose: theory, implementation, and optimization procedures. J Cereb Blood Flow Metab 14:406–422
38. Gunn RN, Gunn SR, Cunningham VJ (2001) Positron emission tomography compartmental models. J Cereb Blood Flow Metab 21:635–652